ELSEVIER

Soil Dynamics and Earthquake Engineering 26 (2006) 363–376

SOIL DYNAMICS AND EARTHQUAKE ENGINEERING

www.elsevier.com/locate/soildyn

Development of Winkler model for static and dynamic response of caisson foundations with soil and interface nonlinearities

Nikos Gerolymos, George Gazetas *

Department of Civil Engineering, National Technical University, Athens, Greece

Accepted 3 December 2005

Abstract

As an extension of the elastic multi-spring model developed by the authors in a companion paper [Gerolymos N, Gazetas G. Winkler model for lateral response of rigid caisson foundations in linear soil. Soil Dyn Earthq Eng; 2005 (submitted companion paper).], this paper develops a nonlinear Winkler-spring method for the static, cyclic, and dynamic response of caisson foundations. The nonlinear soil reactions along the circumference and on the base of the caisson are modeled realistically by using suitable couple translational and rotational nonlinear interaction springs and dashpots, which can realistically (even if approximately) model such effects as separation and slippage at the caisson–soil interface, uplift of the caisson base, radiation damping, stiffness and strength degradation with large number of cycles. The method is implemented in a new finite difference time-domain code, NL-CAISSON. An efficient numerical methodology is also developed for calibrating the model parameters using a variety of experimental and analytical data. The necessity for the proposed model arises from the difficulty to predict the large-amplitude dynamic response of caissons up to failure, statically or dynamically. In a subsequent companion paper [Gerolymos N, Gazetas G. Static and dynamic response of massive caisson foundations with soil and interface nonlinearities—validation and results. Soil Dyn Earthq Eng; 2005 (submitted companion paper).], the model is validated against in situ medium-scale static load tests and results of 3D finite element analysis. It is then used to analyse the dynamic response of a laterally loaded caisson considering soil and interface nonlinearities.

Keywords: Caisson; Winkler model; Soil–caisson interaction; Lateral loading; Cyclic loading; Interface nonlinearities; Sliding; Uplifting

1. Introduction

This paper is part of a sequence by the authors dealing with the lateral response of circular, square and rectangular shaped rigid caissons. In the first paper [2], a Winkler model was developed for the dynamic response of a caisson embedded in an elastic halfspace, and subjected to inertial and kinematic seismic loading. The Winkler spring stiffness and damping parameters were obtained by suitably matching the model response predictions with published results of 3D wave propagation (elastodynamic) analyses. The major limitation of that model is that soil nonlinear behaviour was not been taken into account, and that the caisson assumed to remain in complete contact with the surrounding soil (perfect bonding at the boundaries). However, soil–caisson interaction involves complicated material and geometric nonlinearities such as soil inelasticity, separation (gapping) between the caisson shaft and the soil, slippage at the soil–caisson shaft interface, base uplifting, and perhaps even loss of soil strength (e.g. due to development of excess pore water pressures). Moreover, the waves emanating from the caisson periphery generate radiation damping which is strongly influenced by such nonlinearities. The general problem of a caisson embedded in cohesionless or cohesive soils and subjected to lateral loading is conceptualized in the sketch of Fig. 1. With strong interface nonlinearities a substantially different response emerges.

To compute such nonlinear response (under monotonic and cyclic deformation), the macroscopic Bouc–Wen (BW) model [3,4] has been adapted and extended by the authors [5], and is utilised (as BWGG model) for the normal and shear soil reactions along the caisson perimeter, and for the moment and shear reactive forces at the base. A comprehensive methodology is developed for identification/calibration of the model parameters. In the companion paper no. 3 [1], the capability of the model is investigated through a detailed parametric study, and its predictions are compared with results of in situ monotonic caisson load tests.

* Corresponding author.
E-mail address: gazetas@ath.forthnet.gr (G. Gazetas).

0267-7261/$ - see front matter © 2005 Elsevier Ltd. All rights reserved.
doi:10.1016/j.soildyn.2005.12.002

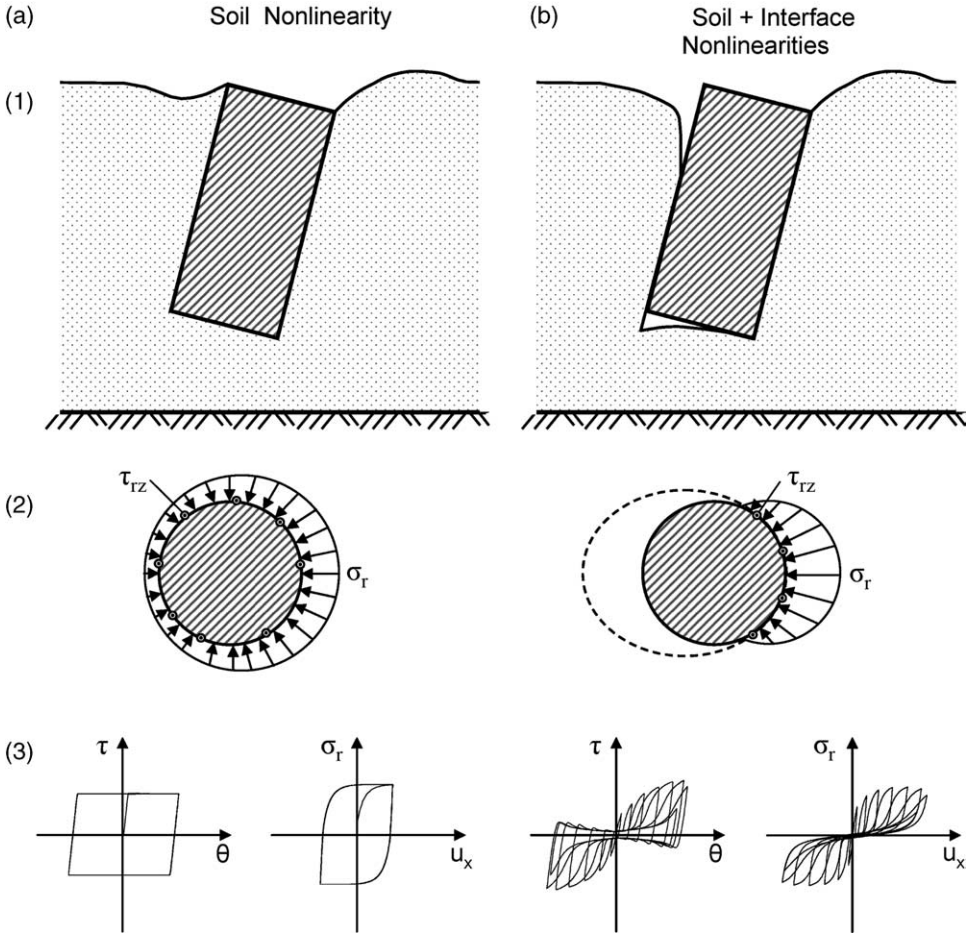

Fig. 1. The general problem of a caisson embedded in a cohesionless (left), and in a cohesive (right) soil, and subjected to lateral loading: (a) only soil inelasticity is involved, and (b) both soil and interface nonlinearities take place. (1) Schematic illustration of the caisson lateral displacement; (2) distributions of the normal and vertical shear tractions around the caisson section, and (3) stress–displacement hysteretic loops at the perimeter of the caisson.

2. Physics of the problem and Winkler multi-spring model

The stress reactions against a laterally displacing caisson are sketched in Fig. 2. The lateral soil resistance (p_x, resultant per unit depth) comprises two horizontal stress components: the radial normal, σ_r, and the tangential shear, $\tau_{r\psi}$, tractions at each depth of the caisson shaft. Their inter-relationship is:

$$p_x(z) = \int_0^{2\pi} (\sigma_r \cos\psi + \tau_{r\psi} \sin\psi) \frac{B}{2} \mathrm{d}\psi \tag{1}$$

Due to the rotation of the caisson vertical shear stresses $\tau_{rz} = \tau_{rz}(\psi)$ develop along the circumference of the caisson. By contrast to piles, for which due to their slenderness such stresses have a negligible effect and are almost invariably ignored in practice, the relatively large diameter and rigidity of caissons make the magnitude of such stresses substantial. And moreover, their contribution to resisting the external loads is significant. Indeed, at every depth, they produce a resisting moment m_θ (per unit depth) about the horizontal axis perpendicular to the direction of loading and passing through the center of the caisson cross-section. This moment is computed as

$$m_\theta(z) = \int_0^{2\pi} \tau_{rz}(\psi) \left(\frac{B}{2}\right)^2 \cos\psi \mathrm{d}\psi \tag{2}$$

where B is the diameter of the caisson.

On the base, the resultant of the shear tractions that act in the radial, τ_{rz}, and in the circumferential, $\tau_{\psi z}$, direction, is given by

$$Q_b = \int_0^{B/2} \int_0^{2\pi} (-\tau_{zr} \cos\psi + \tau_{z\psi} \sin\psi) r \mathrm{d}\psi \mathrm{d}r \tag{3}$$

Finally, the normal reaction σ_z acting at the base of the caisson produce the resisting external moment:

$$M_b = \int_0^{B/2} \int_0^{2\pi} (\sigma_z \cos\psi) r^2 \mathrm{d}\psi \mathrm{d}r \tag{4}$$

In view of all these resisting mechanisms, a static and dynamic Winkler model is developed incorporating *distributed* lateral translational and rotational inelastic springs along the height of the caisson, and *concentrated* (resultant) shear and moment inelastic springs at the base of the caisson. For the dynamic problem viscoplastic dashpots are attached in-parallel

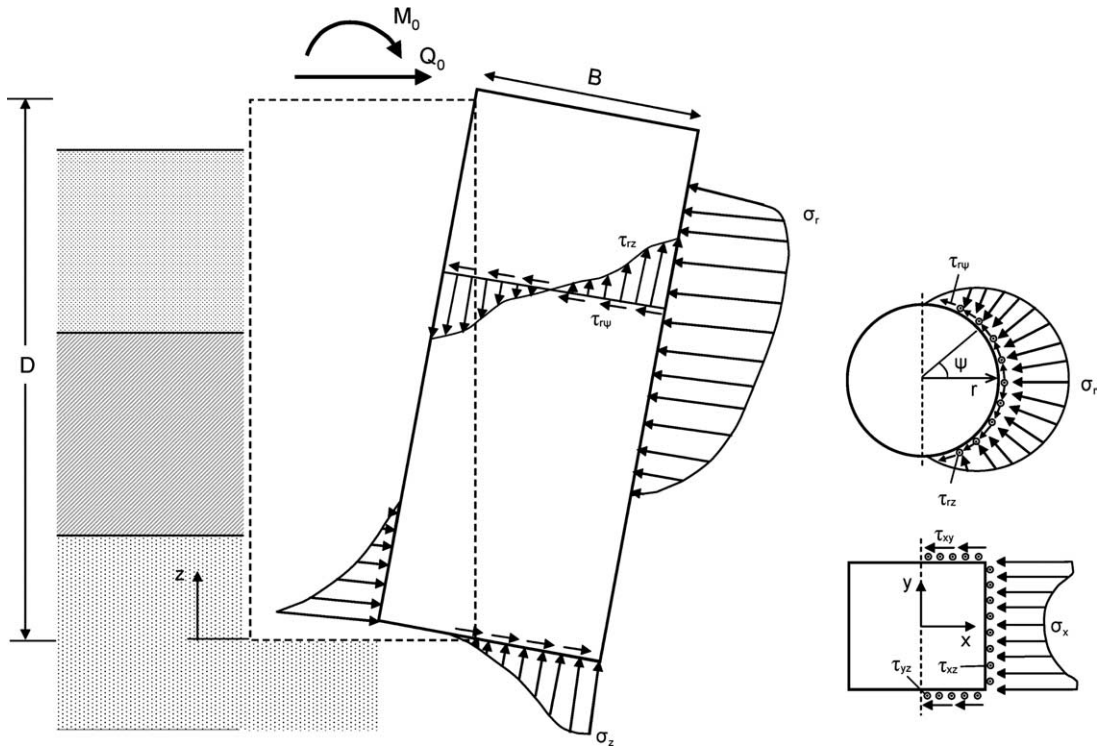

Fig. 2. Stresses at caisson–soil interface, with circular or square plan shape.

with each spring. These four types of springs and dashpots relate the resisting forces acting on the caisson with the resulting deformations, as follows:

- Nonlinear lateral translational springs and dashpots associated with the horizontal soil reaction on the side of the caisson. The separation (gapping) of the caisson from the soil is also modeled with these springs and dashpots. Their initial elastic moduli, k_x and c_x, are determined according to the companion paper [1].
- Nonlinear rotational springs and dashpots associated with the moment produced by the vertical shear stresses on the perimeter of the caisson. Slippage at the caisson–soil interface is also modelled with these springs and dashpots. Their initial elastic moduli, k_θ and c_θ, are also determined according to the first companion paper [1]. However, an important complication arises at large deformations and near failure conditions: the [ultimate] shear tractions (and hence the ultimate rotational spring resistance) stem from the frictional capacity of the interface; as such, they are directly related to the normal tractions, which however, also control the horizontal springs. Hence, rotational and translational spring and dashpot moduli and coupled.
- A nonlinear base shear translational spring and dashpot associated with the horizontal shearing force on the base of the caisson. Their initial elastic moduli are K_h and C_h, determined as for a surface footing on the (underlying the caisson base) elastic halfspace, according to Ref. [2].
- A nonlinear base rotational spring and dashpot associated with the moment produced by normal pressures on the base of the caisson. The uplift at the caisson base is also modeled by this spring and dashpot. Their initial elastic moduli are K_r and C_r, determined as for a surface footing on an elastic halfspace [2]. Again, at ultimate conditions, rotational and shear springs (and dashpots) at the base are coupled, due to the frictional nature of the shearing resistance and hence its dependence on the rotation-related σ_z.

The proposed nonlinear Winkler model is illustrated schematically in Fig. 3.

3. The model: constitutive equations

The lateral soil reaction p_x given in Eq. (1) is expressed as the sum of two components, the hysteretic, p_s, and the viscoplastic, p_d:

$$p_x = p_s + p_d \tag{5}$$

The constitutive relationship for p_s is expressed in the Bouc–Wen fashion [3,4] as

$$p_s = \alpha_x k_x u + (1-\alpha_x) p_y \zeta_x \tag{6}$$

in which: p_s is the resultant in the direction of loading of the normal and shear tractions along the perimeter of the caisson of a unit thickness, u is the horizontal displacement of the caisson at the location of the spring; k_x is the initial stiffness of the translational spring; α_x is a parameter that controls the post-yield stiffness; p_y is the ultimate soil reaction; and ζ_x is a hysteretic dimensionless quantity controlling the nonlinear behaviour of the lateral soil reaction. The latter is governed by

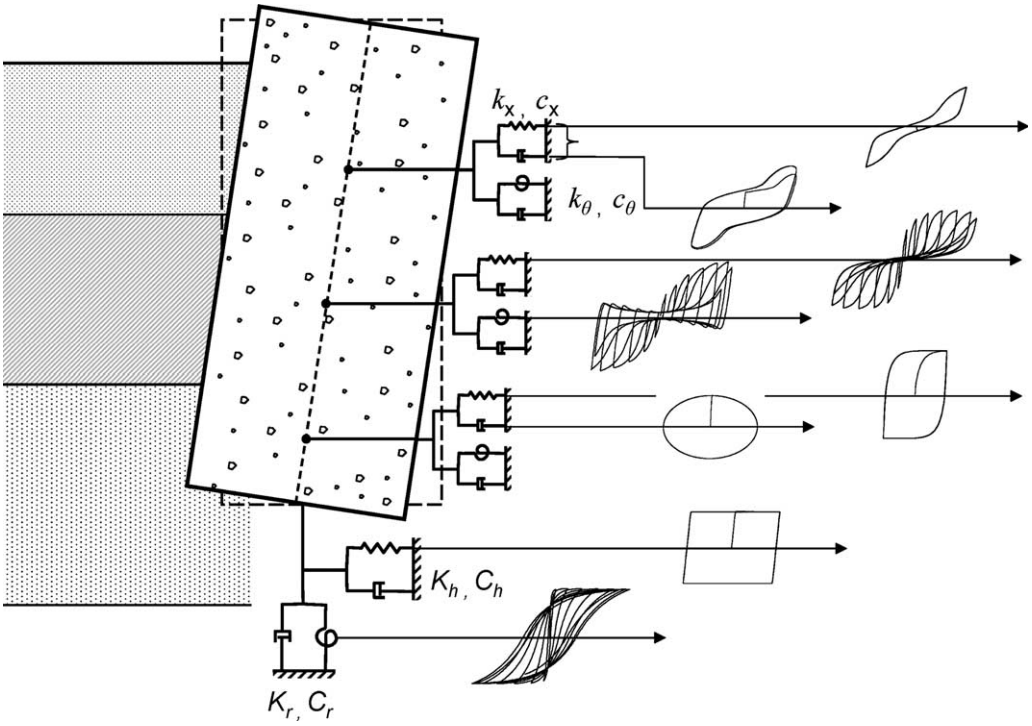

Fig. 3. Nonlinear Winkler model for the analysis of laterally loaded caissons.

the following differential equation with respect to time, t

$$\frac{\mathrm{d}\zeta_x}{\mathrm{d}t} = \lambda_x \frac{h_x}{u_y}\left[\frac{\mathrm{d}u}{\mathrm{d}t} - (1+r_x)\left(b_x \frac{\mathrm{d}u}{\mathrm{d}t}|\zeta_x|^{n_x} + g_x\left|\frac{\mathrm{d}u}{\mathrm{d}t}\right||\zeta_x|^{n_x-1}\zeta_x\right)\right] \tag{7}$$

where

$$h_x \equiv h_x(\zeta_x) = 1 - \zeta_0 \exp\left[-\left(\frac{u_y\zeta_x}{\delta\Delta}\right)^2\right] \tag{8}$$

is the 'pinching factor', for modeling the effect of the gap formation.

In the above equations b_x, g_x, n_x, λ_x, r_x, ζ_0, δ, and Δ are dimensionless quantities which control the shape of the monotonic (backbone) curve, and of the hysteresis loop of the lateral soil reaction versus caisson deflection; $u_y = p_y/k_x$ is the value of lateral displacement at initiation of yielding in the soil at the specific depth. The exact role of each of the above parameters is illustrated in the sequel.

The original idea of the form of Eqs. (6) and (7) was proposed by Bouc [3] and was subsequently extended by Wen [4] and used extensively especially in studies of inelastic structural systems. The form of Eqs. (7) and (8) was developed specifically for the caisson problem studied in this paper. Eq. (7) can be rewritten in an incremental $\mathrm{d}\zeta - \mathrm{d}u$ form by eliminating t:

$$\mathrm{d}\zeta_x = \frac{\lambda_x h_x}{u_y}\{1 - (1+r_x)|\zeta_x|^{n_x}[b_x + g_x \mathrm{sign}(\mathrm{d}u\zeta_x)]\}\mathrm{d}u \tag{9}$$

It is evident that Eq. (9) is of hysteretic rather than viscous type. This means that its solution is not frequency dependent. Different numerical integration techniques can be utilized to solve Eq. (9) such as the central finite difference and the Range-Kutta methods. The explicit scheme of the finite difference method is more suitable when Eq. (9) is to be solved in conjunction with the system (e.g. pile–soil or caisson–soil) equilibrium equations, under the condition that the size of the time step is sufficiently small.

The lateral reaction resulting from the viscoplastic dashpot is given by

$$p_\mathrm{d} = c_x \frac{\partial u}{\partial t}\left[a_x + (1-a_x)\frac{\partial \zeta_x}{\partial u}\right]^{c_{x\mathrm{d}}} \tag{10}$$

where c_x is the dashpot coefficient at small amplitude motions, and $c_{x\mathrm{d}}$ is a viscoplastic parameter which controls the coupling of soil and soil–caisson interface nonlinearity with radiation damping.

As with the lateral reaction, p_x, the resisting moment per unit depth, m_θ, given in Eq. (2), is expressed as the resultant of the hysteretic, m_s, and the viscoplastic, m_d,component

$$m_\theta = m_\mathrm{s} + m_\mathrm{d} \tag{11}$$

where

$$m_\mathrm{s} = m_y \zeta_\theta \tag{12}$$

in which m_y is the ultimate resisting moment at initiation of slippage at the soil–caisson interface at the specific depth. m_y depends on the lateral soil reaction p_s, given in Eq. (6), which varies with time. A methodology for calibrating m_y is presented in the sequel. ζ_θ is the hysteretic dimensionless rotation that controls the nonlinear response of the resisting moment (per

unit depth). The latter is governed by the following differential equation

$$\frac{d\zeta_\theta}{dt} = \lambda_\theta \frac{1}{\theta_y}\left[\frac{d\theta}{dt} - (1+r_\theta)\left(b_\theta \frac{d\theta}{dt}|\zeta_\theta|^{n_\theta} + g_\theta \left|\frac{d\theta}{dt}\right| |\zeta_\theta|^{n_\theta - 1}\zeta_\theta\right)\right] \tag{13}$$

In which θ is the rotation of the caisson, b_θ, g_θ, n_θ, λ_θ, and r_θ are dimensionless quantities which control the shape of the lateral soil reaction versus caisson-deflection hysteresis loop; θ_y is the value of caisson rotation at initiation of slippage at the soil–caisson interface, expressed as a function of the initial stiffness of the rotational spring

$$\theta_y = \frac{m_y}{k_\theta} \tag{14}$$

Eq. (13) is similar in form with Eq. (7) except that there is no term equivalent to h_x.

The viscoplastic component of the resisting moment due to radiation damping is described as

$$m_d = c_\theta \frac{\partial\theta}{\partial t}\left[a_\theta + (1-a_\theta)\frac{\partial\zeta_\theta}{\partial u}\right]^{c_{\theta d}} \tag{15}$$

where c_θ is the damping coefficient at small amplitude motions, and $c_{\theta d}$ is a viscoplastic parameter which controls the coupling of soil inelasticity and slippage at the soil–caisson interface, with radiation damping. It is obvious from Eq. (15) that when sliding occurs the term inside the brackets vanishes, and so does therefore m_d. This means that the system generates no radiation damping from rotational oscillation when slippage at soil–caisson interface takes place—a realistic outcome.

As with p_x and m_θ, the shear force Q_b and overturning moment M_b at the caisson base, given in Eqs. (3) and (4) respectively, are expressed as

$$Q_b = Q_{bs} + Q_{bd} \tag{16}$$

and

$$M_b = M_{bs} + M_{bd} \tag{17}$$

in which the hysteretic components Q_{bs} and M_{bs} are given by

$$Q_{bs} = Q_{by}\zeta_h \tag{18}$$

and

$$M_{bs} = \alpha_r K_r \theta + (1-\alpha_r)M_{by}\zeta_r \tag{19}$$

The hysteretic quantities ζ_h and ζ_r are the solutions of differential equations of identical form as Eqs. (7) and (13) with their own constants and the following meaning of the yield displacement and rotation: $u_{by} = Q_{by}/K_h$ and $\theta_{by} = M_{by}/K_r$. Radiation damping components Q_{bd} and M_{bd} are also governed by equations analogous to Eqs. (10) and (15), respectively.

A delicate point that deserves some discussion is that the resisting stresses acting on the caisson base are represented by springs and dashpots *concentrated at* the centre of the base. However, the pivot point of an oscillating caisson free to rock on a rigid base alternates between the two corner points. Consider for instance that uplifting has occurred at a certain moment in time. Upon re-attachment of the free portion of the base, new forces participate in the dynamic equilibrium and one is expecting the need of a balance of momentum equation [25]. The problem becomes more complex when the caisson is supported on a deformable soil where a smooth transition of the pivot point between the two corners takes place. As it is shown in the sequel, the influence of the pivot point alteration on the resisting forces is *implicitly* considered with our nonlinear 'springs', through the appropriate calibration of the model parameters. Calibration is achieved against results of 3D finite element analysis using the methodology presented in a subsequent section. This is a 'macro-element' type of approach, capturing the overall caisson base response. A similar in concept macro-element has also been developed by Cremer et al. [26] in modelling the dynamic behaviour of a shallow strip foundation under seismic action.

Eqs. (6)–(8) are a generalization and extension of a model originally proposed by Bouc [3] subsequently extended by Wen [4], Baber and Wen [7] and Baber and Noori [8], and used extensively in random vibration studies of degrading-pinching inelastic structural systems, and later in modeling the response of seismic isolation bearings [9]. Applications in soil dynamics include the probabilistic soil response studies by Pires [10], Loh et al. [11] and Gerolymos and Gazetas [5,6]. To our knowledge the first application to soil–pile interaction problems under static condition was made by Trochanis et al.

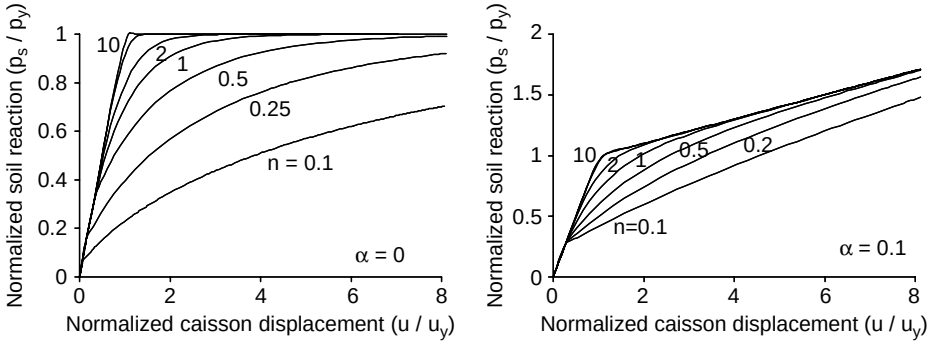

Fig. 4. Normalized soil reaction–caisson displacement curves to monotonic loading for selected values of parameter n, computed with the proposed model for caissons. $a=0$ and 0.1.

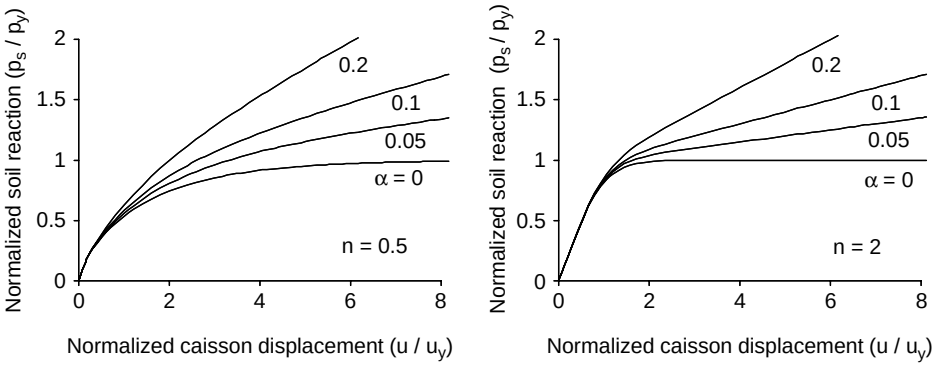

Fig. 5. Normalized soil reaction–caisson displacement to monotonic loading for selected values of post-yielding parameter α computed with the proposed model for caissons. $n=0.5$ and 2.

[12], and under dynamic loads by Badoni and Makris [13] and Gerolymos and Gazetas [6].

A methodology is developed in the sequel for calibrating the parameters of the model. Special attention is given to modeling the separation and slippage at the caisson–soil interface, as well as the base uplifting.

4. Key parameters and capabilities of the model

For a better understanding of the constitutive relations used in modeling caisson–soil interaction to lateral loading, a brief outline is presented herein of the parameters, capabilities, and limitations of the model.

4.1. Parameters for monotonic loading

The parameter n (n_x for the lateral soil reaction, and n_θ for the resisting moment, per unit depth) controls the rate of transition from the elastic to the yield state. A large value of n (greater than 10) models approximately a bilinear hysteretic curve; decreasing values of n lead to smoother transitions where plastic deformation occurs even at low loading levels. Fig. 4 illustrates the role of n on the monotonic loading curve.

The parameter α (α_x for the lateral soil reaction, and α_θ for the resisting moment, per unit depth) is the ratio of post-yield to initial elastic stiffness. Monotonic loading curves for different values of α and for constant value of n are presented in Fig. 5. The parameters n and α are properly calibrated to matching any lateral '$p-y$' and vertical '$t-z$' curve, such as those proposed by Matlock [14] and Reese [15] for piles Fig. 6.

4.2. Parameters for unloading–reloading

Parameters b (b_s for the horizontal reaction, b_θ for the resisting moment, per unit depth, and b_r for the base moment) and g (g_x, g_θ, and g_r) control the shape of the unloading–reloading curve. As is shown in Fig. 7 there are four basic hysteretic shapes depending on the relation between b and g. When $b=g=0.5$, the stiffness upon reversal equals the initial stiffness, and the Masing criterion is recovered. In the special case $b=1$ and $g=0$, the hysteretic loop collapses to the monotonic loading curve (nonlinear but elastic behavior,

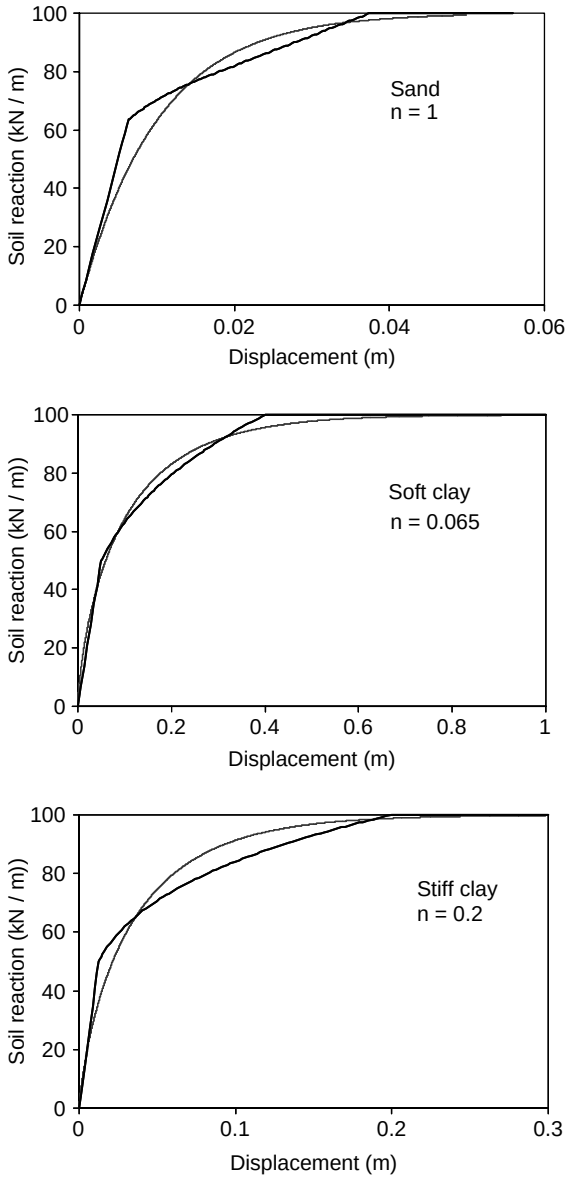

Fig. 6. Comparison of $p-y$ curves computed with the proposed model for caissons (smooth lines), and proposed by Reese and Matlock [14,15] (three lines) for sand, soft clay, and stiff clay.

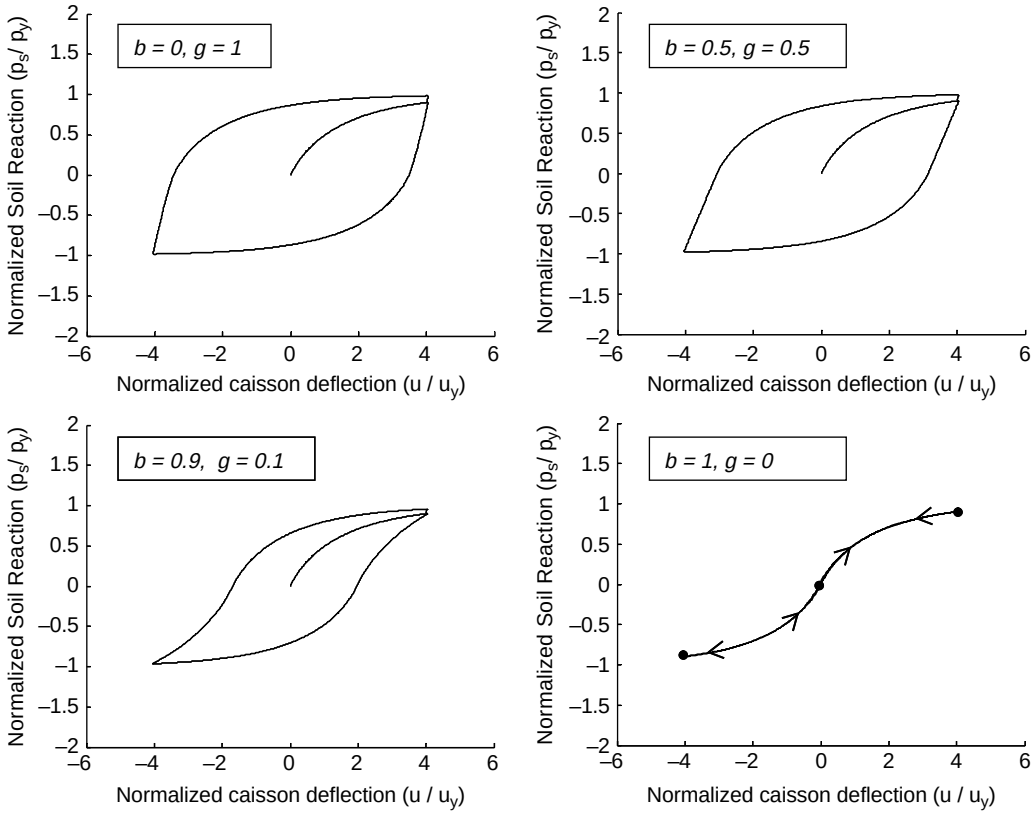

Fig. 7. Hysteresis loops of normalized soil reaction–caisson displacement for different values of b and g, and $n=1$. The Masing criterion for unloading–reloading is obtained for $b=0.5$ and $g=0.5$.

appropriate for geometric nonlinearities but not for material nonlinearity).

4.3. Parameters for stiffness and strength degradation with cyclic loading

The model can reproduce stiffness and strength degrading behavior. Stiffness decay is controlled by the parameter λ (λ_x, λ_θ and λ_r). Prescribing λ to be an increasing function of time will model stiffness decay. λ can be expressed as a function of the dissipated hysteretic energy and/or the cumulative displacement or rotation ductility. Its influence on the hysteretic loops is depicted in Fig. 8. The proposed model could also simulate strength degradation with cyclic loading. This is achieved with parameter r (r_x, r_θ, and r_r). Increasing r, reduces the soil strength in proportion to $(1+r)$. Parameter r can be prescribed as an increasing function of dissipated energy, according to

$$r_x(t) = \beta[(1-\alpha_x)p_y \int_0^t \zeta_x(u,t)\dot{u}(t)\mathrm{d}t]^\gamma \tag{20}$$

where β and γ are parameters determined from experimental data. As an example of the capabilities of the model, Fig. 9 depicts hysteresis loops of lateral soil reaction versus displacement, for a caisson in stiff clay experiencing gapping and displacement-controlled strength degradation.

4.4. Parameters for separation and slippage between caisson and soil

Gap opening up around the caisson (particularly significant with stiff clays), and slippage at the soil–caisson interface (significant for both sands and clays), are treated as coupled phenomena. Gapping is implemented through the pinching function $h_x=h_x(\zeta_x)$ given in Eq. (8). The continuous nature of the pinching function produces smooth hysteresis loops with gradual transition from almost zero to maximum stiffness. The parameter δ in Eq. (8) controls the gap growth during the

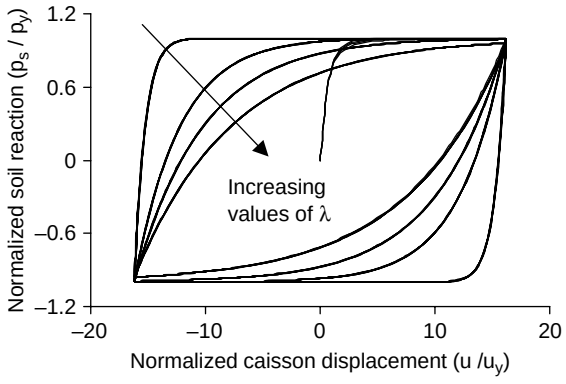

Fig. 8. Effect of parameter λ on force–displacement hysteresis loops.

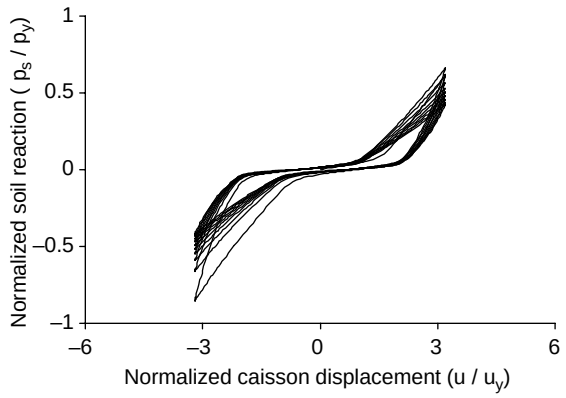

Fig. 9. Hysteretic component of a typical soil reaction on a caisson in stiff clay with gapping effect and displacement-controlled strength deterioration, computed with the proposed model for caissons.

response of the caisson, while the parameter ζ_0 controls the 'sharpness' of the separation. In this equation, Δ is either the maximum or the minimum attained displacement, depending on whether the displacement u is positive or negative, respectively. In the absence of experimental data, the calibration of parameters ζ_0 and δ should be based on the following rule

$$\zeta_x(t) = \begin{cases} 0, & -\Delta(t) < u(t) < \Delta(t) \\ 1, & u(t) = \Delta(t) \end{cases} \tag{21}$$

It has been found that for $\zeta_0 = 0.99$ and $\delta = 0.054$, the above criterion is approximately fulfilled. Fig. 10 portrays a lateral soil reaction versus displacement loop with gapping effect, computed from the system of Eqs. (6)–(8), and (21).

Having calibrated the parameters of the pinching function, h_x, the next step should be to determine the conditions under which separation occurs. Two conditions must be satisfied simultaneously: (i) the lateral extensional stress p_s [Eq. (6)] at a particular depth on the interface becomes larger than the compressive horizontal earth pressure at rest, σ_{h0}, *and* (ii) the cavity formed around the caisson is stable. Mathematically, separation occurs when

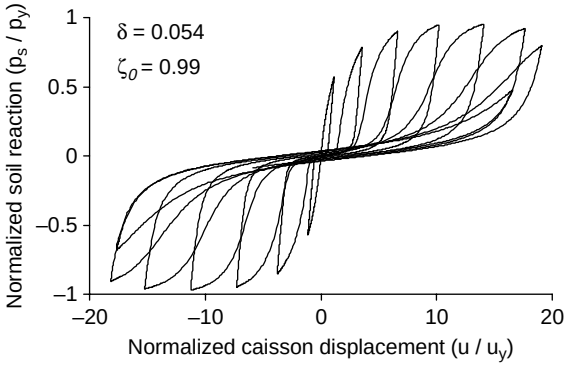

Fig. 10. Simulation with the proposed model of the hysteretic component of soil reaction on a caisson experiencing gapping.

$$\begin{cases} \sigma_{h0} B < |p_s| \\ \sigma_{h0} < f(c,\varphi) \end{cases} \tag{22}$$

in which $f(c,\phi)$ is a function of the soil strength parameters ($c =$ the cohesion, and $\phi =$ the friction angle) related to the stability of the cavity. In the absence of a more rigorous solution, $f(c,\phi)$ can be derived through the application of cavity expansion theory [16]. For example, for soil obeying the Mohr–Coulomb yielding criterion,

$$f(c,\varphi) = \frac{2c\cos\varphi}{(1-\sin\varphi)(3K_0-1)} \tag{23}$$

where K_0 is coefficient of earth pressure at rest.

Slippage occurs when the shear stress at the interface becomes larger than the ultimate shear stress (friction). The developed shear stress

$$\tau_r = \sqrt{\tau_{ry}^2 + \tau_{rz}^2} \tag{24}$$

is the resultant of the horizontal component $\tau_{r\psi}$ which contributes to the lateral soil reaction, p_s, and the vertical component τ_{rz} which contributes to the resisting moment, m_s, per unit depth. The ultimate shear stress Mohr–Coulomb yield criterion. Summarising, for initiation of slippage at a particular depth, the following rule must be satisfied at every point of the interface

$$|\tau_r| = c_{\text{int}} + (\sigma_{h0} + |\sigma_r|)\tan\delta_{\text{int}} \tag{25}$$

where δ_{int} is the peak friction angle between caisson and soil. Once slippage has occurred, Eq. (25) transforms to

$$|\tau_r| = (\sigma_{h0} + |\sigma_r|)\tan\delta_{\text{int, res}} \tag{26}$$

in which $\delta_{\text{int,res}}$ is the residual friction angle at the interface (residual cohesion ≈ 0). Finally, during separation of the caisson from the soil the shear stresses vanish ($\tau_r = 0$). The method to relate the ultimate shear stress with the ultimate resisting moment m_y, which is an important consideration of the proposed model for caissons, is presented in the sequel.

4.5. Parameters for caisson base uplifting

Base uplifting may have an appreciable effect on the dynamics of caisson foundations. For relatively shallow caissons in which the base contributes significantly to the overall stiffness of the foundation, uplifting may even dominate the response. The problem becomes more complicated due to the interplay between base uplifting and plastification of the underlying soil. This interplay is elucidated with the help of Fig. 11.

The problem shown in this figure is that of a circular footing supported on clay of constant undrained shear strength with depth. The footing is subjected to monotonic moment loading M at its center under constant vertical load N, until the complete failure of the footing–soil system. The figure shows comparison between M–θ monotonic curves computed with 3D finite element analysis [27] and predicted with the proposed model with appropriate calibration of parameter n_r. The

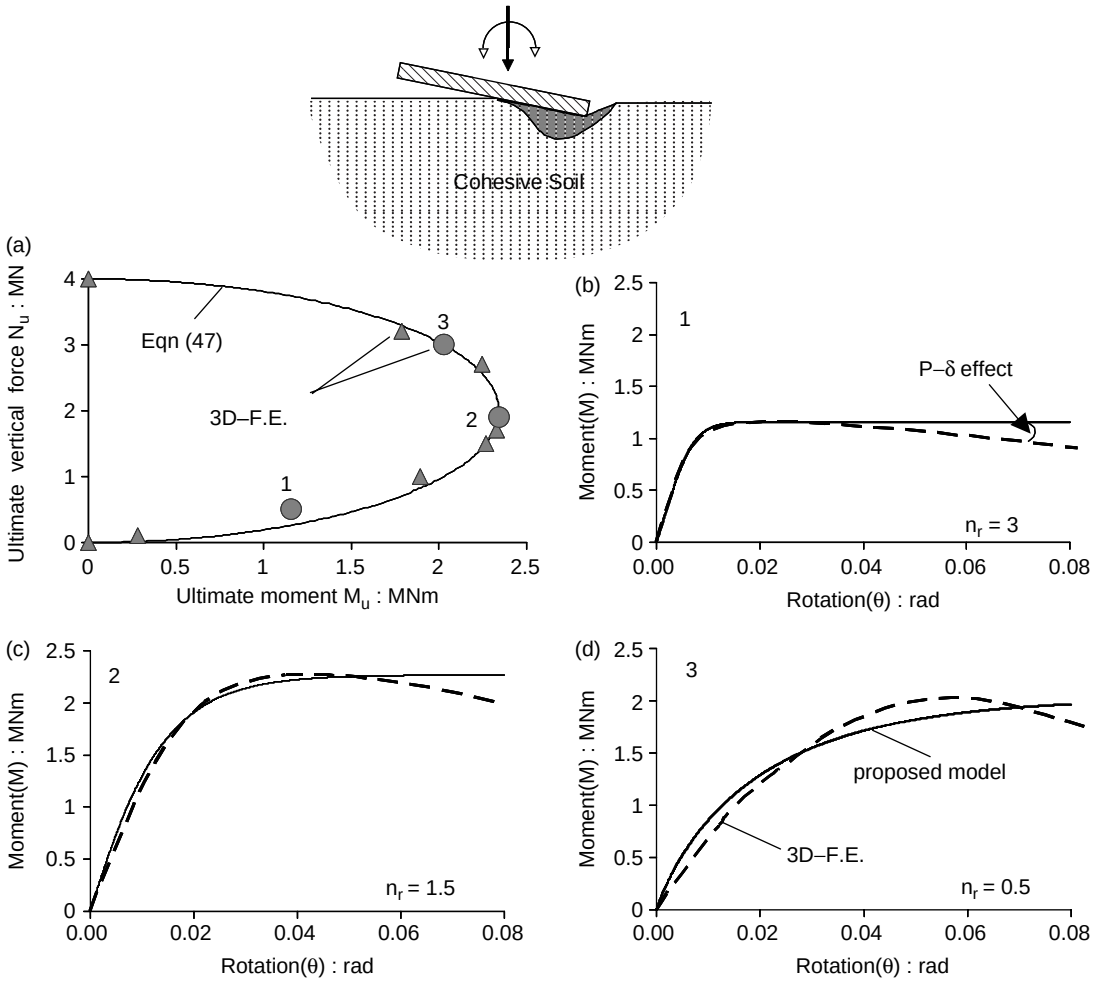

Fig. 11. (a) Vertical force–moment interaction diagrams for a rigid square foundation on a clayey soil, computed from Eq. (47) (solid line), and derived from 3D finite element analysis (triangles and circles, Gazetas and Apostolou 2004). (b–d) Associated to the interaction diagrams M–θ curves, computed from the proposed model for caissons (solid lines) and derived from finite element analysis (dotted lines, Gazetas and Apostolou 2004). The curves correspond to factors of safety for central static vertical loading, FS = 8 (circle 1), 2.1 (circle 2),and 1.3 (circle 3). The negative post-yielding slope of the M–θ curves computed with the finite element model, is due to the $P-\delta$ effect.

monotonic M–θ curves correspond to specific points on the vertical force–moment interaction diagram of the footing, calculated with the finite element model, also shown in the same figure. Each of the three points is associated with a different factor of safety (under static vertical loading): FS = 8.0, 2.1, and 1.3.

As shown in this figure, the transition from the elastic to the fully plastic region is smoother for curves corresponding to small factors of static safety, say FS < 2, where the soil plastification dominates, than those for FS > 2 where uplifting dominates. In the case of an almost rigid foundation soil, the M–θ curve approaches a bilinear (but elastic) behaviour (with a horizontal branch). Summarizing, parameter n_r can be expressed as an increasing function of the static safety factor to vertical loading. In the absence of results from a push-over analysis, the following guidelines for calibrating n_r are appropriate: for large values of the factor of safety (f.e. FS > 10), n_r shall be taken equal to 10. For values of FS = 8, FS = 2 and FS = 1, n_r is taken equal to 3, 1.5 and 0.5, respectively. For intermediate values of the factor of safety a linear interpolation would suffice.

The next step is to calibrate the parameter b_r for matching the observed unloading–reloading behaviour. To this end, Fig. 12 presents a qualitative comparison between experimental and calculated M–θ hysteresis loops for a soil–footing system. Three particular cases of the soil–footing system are examined. Cases (a) and (c) are the two extremes: (a) of a very hard foundation soil, or alternatively of a footing with large static factor of safety (e.g. FS > 8), and (c) of very soft foundation soil, or alternatively a footing with small factor of safety (e.g. FS < 2). Case (b) is intermediate: of a medium stiff foundation soil, or alternatively of a footing with a factor of safety between 2 and 4—as is most frequently the case in practice.

Rotation of the footing in case (a) is possible only after uplifting initiates (with or without structural yielding). The corresponding M–θ curves for several cycles of loading–unloading–reloading practically coincide with the monotonic

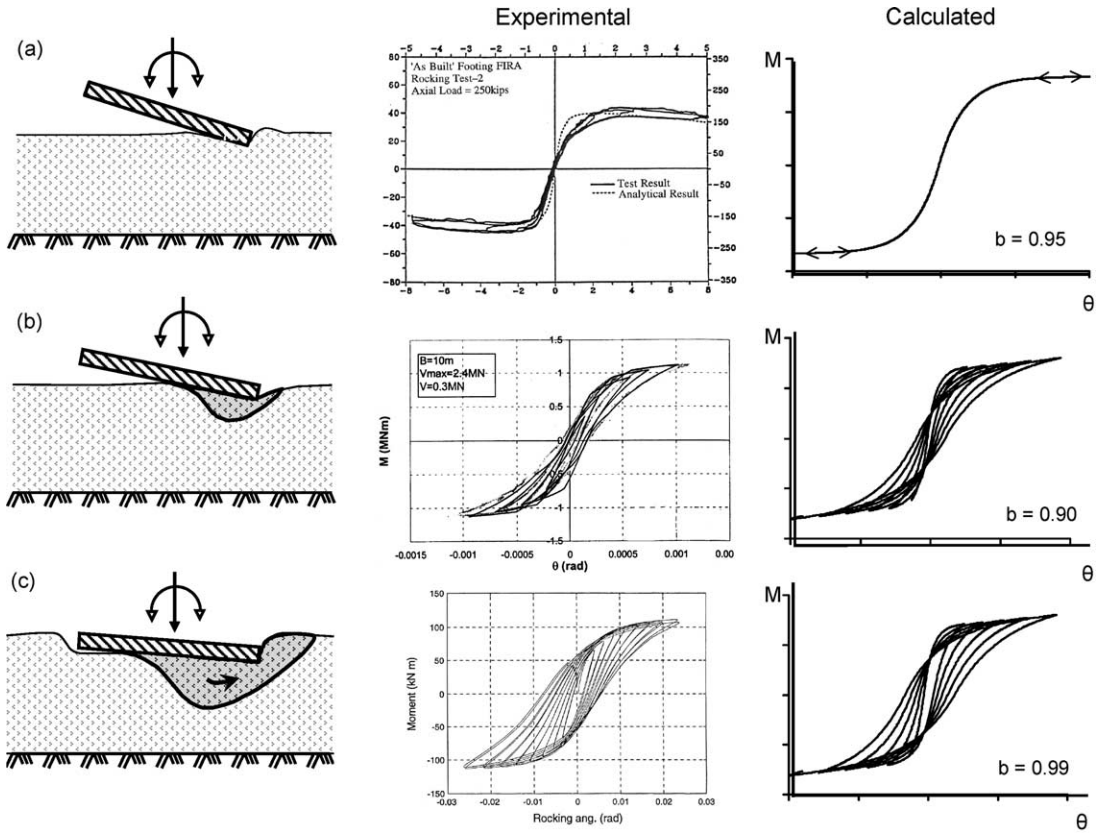

Fig. 12. Experimental and calculated moment–rotation (M–θ) hysteresis loops of a soil–footing interaction system. (a) Uplift on very stiff soil accompanied with slight structural yielding. (b) Uplifting with limited soil plastification; uplift is the prevailing failure mechanism, and (c) uplifting with extensive soil plastification; soil yielding is the predominant failure mechanism. The comparison between experimental M–θ loops and those calculated with the proposed model for caissons is *only* qualitative.

curve—indicative of *nonlinear* but *elastic* behavior. Such a behavior is the result of *geometric* (not material) nonlinearity. The tiny hysteresis loops in the experiment are due to some structural yielding in the footing; such yielding is unlikely to occur with the caisson—hence the single M–θ line of the calculated response (for $n_r = 10$).

The behaviour of case (c), footing on very soft soil, is typical of cyclic behaviour dominated by extensive soil plastification with minimal uplifting. Bearing capacity exceedance mechanisms are mobilized alternately under the two edges of the footing, in each direction of loading. Naturally, hysteresis loops are now substantial, reflecting the hysteretic energy dissipation in the soil.

For the intermediate case (b), the M–θ response reveals that both nonlinear-elastic base uplifting and inelastic soil plastification take place simultaneously. The hysteresis loops are of moderate size reflecting a moderate degree of hysteretic dissipation of energy in soil. It is interesting to observe in the plots of this figure that the stiffer is the foundation soil, the milder is the reversal stiffness of the soil-foundation system, and the narrower is the corresponding hysteretic loop. This type of behaviour is quite realistically captured with the proposed model, by expressing parameter b_r as an *increasing* function of the static vertical factor of safety against bearing capacity failure. Note also that the reversal stiffness becomes milder as the amplitude of the imposed rotation increases. This can also be modeled by expressing the parameter λ_r as a *decreasing* function of the rotation 'ductility' (θ/θ_y).

4.6. Stiffness parameters

The methodology for calculating the small-amplitude subgrade moduli of the distributed (along the height of the caisson) and the concentrated (at the base of the caisson) springs, as well as the dashpot coefficients, is discussed thoroughly in the companion paper [1]. For example, the translational and rotational distributed static spring stiffnesses for a cylindrical-shaped caisson are

$$k_x = 1.60\left(\frac{D}{B}\right)^{-0.13} E_s \tag{27}$$

and

$$k_\theta = 0.85\left(\frac{D}{B}\right)^{-1.71} E_s D^2 \tag{28}$$

while the concentrated springs at the base are obtained without modification from the theory of surface foundations on

homogeneous half-space [28–30]

$$K_h = \frac{2E_s B}{(2-\nu_s)(1+\nu_s)} \tag{29}$$

and,

$$K_r = \frac{E_s B^3}{1-\nu_s^2} \tag{30}$$

accepting the theoretical (numerically verified) arguments by Randolph and Wroth [31].

4.7. Parameters of ultimate resistance

4.7.1. Along the caisson shaft

A methodology is presented in this section for calculating: (i) the ultimate lateral soil reaction p_y and ultimate resisting moment m_y, per unit depth along the caisson, and (ii) the shear Q_y and moment M_y capacities at the base of the caisson.

Referring to Fig. 2 and to Eq. (1), the real part of p_s of the lateral soil reaction p_x is composed of two components as follows

$$p_s = p_n + p_t \tag{31}$$

where p_n and p_t are the integrated resultants of the normal and horizontal shearing stresses, respectively, acting on the periphery of the caisson. Assuming that contact between caisson and soil is not maintained on the back side of the caisson at a specific depth

$$p_n = \int_{-\pi/2}^{\pi/2} \sigma_r \frac{B}{2} \cos\psi \mathrm{d}\psi \tag{32}$$

and

$$p_t = \int_{-\pi/2}^{\pi/2} \tau_{r\psi} \frac{B}{2} \sin\psi \mathrm{d}\psi \tag{33}$$

The ultimate resisting moment per unit depth, m_y, is expressed as a function of p_n according to

$$m_y = (c_{\mathrm{int}} B + |p_n| \tan\delta_{\mathrm{int}}) \frac{B}{2} \tag{34}$$

For the distribution of the normal stress, σ_r, a cosine function is adopted for the variation around the circumference

$$\sigma_r = \sigma_{r0} \cos\psi \tag{35}$$

where σ_{r0} is the amplitude at $\psi = 0$. Substitution of Eq. (35) into Eq. (32) yields

$$p_n = \frac{\pi}{4} B \sigma_{r0} \tag{36}$$

Referring to Eq. (25) and setting $\sigma_{h0} = 0$, the ultimate shear strength at the caisson–soil interface is

$$\tau_r = c_{\mathrm{int}} + \sigma_r \tan\delta_{\mathrm{int}} \tag{37}$$

Since at failure it is the magnitude of *the vector resultant* of $\tau_{r\psi}$ and τ_{rz} that must equal the limiting, τ_r, the following distributions have been assigned as a first approximation to these stresses

$$\tau_{r\psi} = \tau_r \sin\psi \tag{38}$$

and

$$\tau_{rz} = \tau_r \cos\psi \tag{39}$$

Substituting Eqs. (35), (37), and (38) into Eq. (33) yields

$$p_t = \left(\frac{\pi c_{\mathrm{int}}}{4} + \frac{1}{3} \sigma_{r0} \tan\delta_{\mathrm{int}} \right) B \tag{40}$$

Comparing Eq. (40) with Eq. (36) for typical values of c_{int} and δ_{int}, reveals that p_t is only a small fraction (15–20%) of the lateral soil reaction p_s. Accordingly, in Eq. (34) p_n could be replaced with p_s, without any significant loss of engineering accuracy.

A variety of analytical or semi-analytical expressions can be adopted to estimate the ultimate lateral soil reaction p_y. Among others, Duncan and Evans [17] recommended the following approximate equation for the maximum (passive) lateral resistance of $c-\phi$ soils, which is the most preferred in practice, thanks to its simplicity and compatibility with experimental results

$$p_y = C_p \left[2c \tan\left(45 + \frac{\varphi}{2}\right) + \gamma_s z \tan^2\left(45 + \frac{\varphi}{2}\right) \right] B \tag{41}$$

in which C_p is the correction factor accounting for the 3D effect of the passive wedge formed in front of the caisson,

$$C_p = \begin{cases} 1.5, & 0 < \varphi < 15^\circ \\ \varphi/10, & \varphi \geq 15^\circ \end{cases} \tag{42}$$

The reader should recall that for laterally loaded piles, the widely adopted value for C_p is 3 [18].

4.7.2. At the caisson base

The second task of this section is to determine the moment capacity M_{by} at the base of the caisson. This can be achieved through three different alternative approaches: (i) with an elastoplastic Winkler spring model, (ii) with a 3D finite element elastoplastic analysis, and (iii) with the results of experimental (centrifuge or medium- and large-scale) tests. The result of such analyses are cast in the form of 'interaction' curves for combined ultimate (M_u, Q_u, N_u) loading ('*failure equations*').

With the Winkler model, the FEMA manual 273/274 [19] and Allotey et al [20] give

$$M_{by} \approx \frac{N_b}{2} \left(B - \frac{N_b}{q_{\mathrm{ult}}} \right) \tag{43}$$

where N_b is the vertical force acting on the caisson base, and q_{ult} is the ultimate bearing pressure of a surface foundation supported on a soil with the properties of the actual soil below the base of the caisson, in central loading.

With a 3D finite element elastoplastic analysis for circular foundations with uplift, Taiebat and Carter [21] as well as Murff [22], Bransby and Randolph [23], developed the

following '*interaction*' equation,

$$\left(\frac{2N_b}{N_{bu}}-1\right)^2+\left(\frac{M_{by}}{M_{bu}}\right)^2-1=0 \tag{44}$$

in which $N_{bu}(=q_{\text{ult}}\times\text{base area})$ and M_{bu} are the ultimate vertical force and overturning moment, respectively, at the caisson base [24]. Closed-form solutions are not provided for M_{bu} in the literature, except for the interesting particular case of circular foundation on undrained clay, for which Taiebat and Carter [21] derived the following expression

$$M_{bu}=\frac{\pi}{5}B^3S_u \tag{45}$$

in which S_u is the clay undrained shear strength. Eq. (45) is alternatively derived from Eq. (4) by assuming sinusoidal distribution of the normal stress σ_z, and setting its maximum value, σ_{z0}, equal to $5S_u$ which is approximately the bearing capacity of circular footing. Substituting Eq. (45) into Eq. (44), leads to

$$M_{by}=\frac{\pi}{5}B^3S_u\sqrt{1-\left(\frac{2N_b}{N_{bu}}-1\right)^2} \tag{46}$$

Evidently, to calculate M_{by} from Eq. (46) the vertical load acting at the caisson base N_b should be known. N_b is only a fraction of the external vertical load N_0 applied atop the caisson. A substantial part of N_0 is undertaken by the sidewalls. We propose that N_b could be estimated from the following self-explanatory expression

$$N_b\approx N_0-\min\left(\frac{K_{z,\text{ emb}}-K_{z,\text{ sur}}}{K_{z,\text{ emp}}}N_0,\pi DB\tau_u\right) \tag{47}$$

in which $K_{z,\text{emb}}$ and $K_{z,\text{sur}}$ are the vertical stiffnesses of the caisson and the caisson base, respectively, and τ_u the ultimate shear resistance mobilized at the caisson perimeter, in vertical loading. (For clay under undrained conditions, τ_u, is a fraction, β, of the undrained shear strength S_u; usually $0.25<\beta<1$ depending mainly on the value of S_u itself.)

Shear failure at the base of the caisson is usually characterized by sliding at the base–soil interface rather than failure of the foundation soil, Q_{by} is therefore estimated as

$$Q_{by}=N_b\tan\varphi_b \tag{48}$$

where ϕ_b is the angle of friction at the soil–base interface.

4.8. Parameters for radiation damping (viscoplastic approach)

The proposed model is capable of capturing the (unavoidable) coupling between hysteretic and radiation damping with a certain degree of realism. As shown in Eqs. (10) and (15), the dashpot force is expressed as a function of the first derivative of ζ_x (or ζ_θ) with respect to caisson displacement u (or rotation θ), which controls the soil hysteretic response around the pile. The viscoplastic parameters $c_{x\text{d}}$ and $c_{\theta\text{d}}$, controlling the influence of soil hysteretic response on radiation damping, range from 0 to 0.5. When $c_{x\text{d}}$ (or $c_{\theta\text{d}}$)$=0$, then Eqs. (10) and (15) reduce to the linear (small-amplitude) dashpot equation

$$p_{\text{d}}=c_x\frac{\partial u}{\partial t} \tag{49}$$

and

$$m_{\text{d}}=c_\theta\frac{\partial\theta}{\partial t} \tag{50}$$

The larger the value of c_{s}, the more representative the dashpot for soil–pile interaction when high-frequency waves are emitted from the pile periphery. Fig. 13 shows typical loops of soil reaction (normalized to the ultimate soil resistance p_y), versus caisson displacement (normalized to the yield displacement u_y), computed with the proposed model for different values of parameter $c_{x\text{d}}$. The associated viscoplastic components are also presented in this figure. Similar curves for soil reaction with gapping effect are depicted in Fig. 14. Notice the profound reduction in radiation damping either when gapping occurs, or when the ultimate soil resistance is being reached. Paradoxically, the opposite is observed when a purely viscoelastic approach for the radiation damping is adopted ($c_{x\text{d}}=0$).

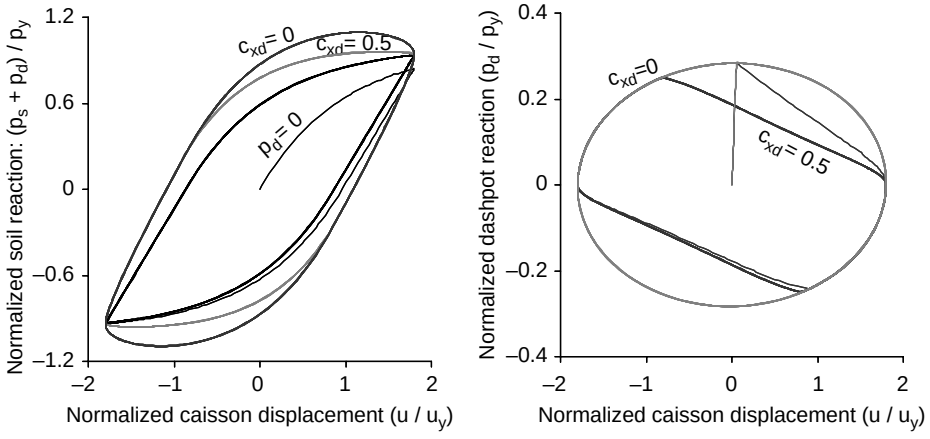

Fig. 13. Left: normalized soil reaction–caisson displacement loops for selected values of viscoplastic parameter $c_{x\text{d}}$ computed with the proposed model for caissons. Right: the associated viscoelastic ($c_{x\text{d}}=0$) and viscoplastic ($c_{x\text{d}}=0.5$) component of lateral soil reaction (dashpot reaction).

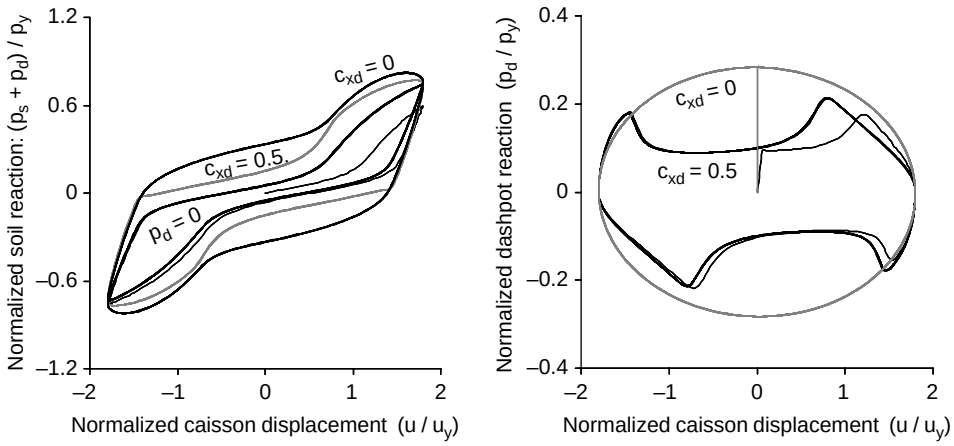

Fig. 14. Left: normalized soil reaction–caisson displacement loops with gapping effect, for selected values of viscoplastic parameter c_{xd} computed with the proposed model for caissons. Right: the associated viscoelastic ($c_{xd}=0$) and viscoplastic ($c_{xd}=0.5$) component of lateral soil reaction (dashpot reaction).

5. Conclusion

A nonlinear Winkler model is presented for the static and inertial response of rigid caisson foundations. The model is an extension of the four-type spring model for the elastic response analysis of caissons, outlined in Part I article. To model the nonlinear reaction of the soil with realism we develop the '*BWGG interaction springs and dashpots*' model, which can capture such effects as: soil failure, separation and gapping of the caisson from the soil, radiation damping, and loss of strength and stiffness (e.g. due to material softening and/or pore-water pressure generation). The coupling of hysteretic and radiation damping is also modeled in a realistically simplified way. A simplified but efficient methodology is then developed for calibrating the model parameters.

References

[1] Gerolymos N, Gazetas G. Static and dynamic response of massive caisson foundations with soil and interface nonlinearities—validation and results. Soil Dyn Earthq Eng, in press, doi: 10.1016/j.soildyn.2005.12.001.

[2] Gerolymos N, Gazetas G. Winkler model for lateral response of rigid caisson foundations in linear soil. Soil Dyn Earthq Eng, in press, doi: 10.1016/j.soildyn.2005.12.003.

[3] Bouc R. Modele mathematique d' hysteresis. Acustica 1971;21:16–25 [in French].

[4] Wen YK. Method for random vibration of hysteretic systems. J Eng Mech ASCE 1976;102:249–63.

[5] Gerolymos N, Gazetas G. Constitutive model for 1D cyclic soil behaviour applied to seismic analysis of layered deposits. Soils Found 2005;45(3): 147–59.

[6] Gerolymos N, Gazetas G. Phenomenological model applied to inelastic response of soil–pile interaction systems. Soil Found 2005; 45(4):119–32.

[7] Baber TT, Wen YK. Random vibration of hysteretic degrading systems. J Eng Mech ASCE 1981;107:1069–87.

[8] Baber TT, Noori MN. Random vibration of degrading systems with pinching hysteresis. ASCE J Eng Mech Div 1985;III(8):1010–26.

[9] Constantinou MC, Mokha A, Reinhorn AM. Teflon bearings in base isolation. Part 2. Modeling. J Struct Eng ASCE 1990;116(ST2): 455–74.

[10] Pires JA, Ang AHS, Katayama I. Probabilistic analysis of liquefaction. Proceedings of fourth international conference on soil dynamic and earthquake engineering, Mexico; 1989.

[11] Loh CH, Cheng CR, Wen YK. Probabilistic analysis of liquefaction. Proceedings of fourth international conference on soil dynamic and earthquake engineering, New Zealand; 1995.

[12] Trochanis A, Bielak J, Christiano P. Simplified model for analysis of one or two piles. J Geotech Eng ASCE 1994;120:308–29.

[13] Badoni D, Makris N. Nonlinear response of single piles under lateral inertial and seismic loads. Soil Dyn Earthq Eng 1995;15:29–43.

[14] Matlock H. Correlations for design of laterally loaded piles in soft clay. Paper No. OTC 1204. Proceedings, second annual offshore technology conference, vol. 1, Houston, Texas; 1970. p. 577–94.

[15] Reese LC, Cox WR, Koop FD. Field testing and analysis of laterally loaded piles in stiff clay. Paper no. OTC 2312. Proceedings, seventh offshore technology conference, vol. II, Houston, Texas; 1975. p. 672–90.

[16] Yu HS, Rowe RK. Plasticity solutions for soil behaviour around contracting cavities and tunnels. Int J Numer Anal Methods Geomech 1999;23:1245–79.

[17] Duncan JM, Evans Jr LT, Ooi PSK. Lateral load analysis of single piles and drilled shafts. J Geotech Eng Div ASCE 1994;120(5):1018–33.

[18] Broms BB. Lateral resistance of piles in cohesionless soils. J Soil Mech Found Div ASCE 1964;90(3):123–56.

[19] FEMA 356/ASCE. Seismic rehabilitation prestandard. Fed Emerg Manage Agency; November 2000.

[20] Allotey N, El Naggar MH. Analytical moment–rotation curves for riged foundations based on a Winkler model. Soil Dyn Earthq Eng 2003;23(5): 367–81.

[21] Taiebat H, Carter JP. Numerical studies of the bearing capacity of shallow footings on the cohesive soil subjected to combined loading. Geotechnique 2000;50(4):409–18.

[22] Murff JD. Limit analysis of multi-footing foundation sytems. In: Siriwardane HJ, Zaman MM, editors. Proceedings of the international conference on computer methods and advanced geomechanics, Morgantown. Rotterdam: Balkema; 1994 p. 233–44.

[23] Bransby MF, Randolf MF. Combined loading of skirted foundations. Geotechnique 1998;48:637–55.

[24] Poulos HG, Carter JP, Small JC. Foundations and retaining structures—research and practice. Proceedings of 15th international conference of soil mechanics and geotechnical engineering, Istanbul, vol. 4; p. 1–80.

[25] Makris N, Roussos YS. Rocking response of rigid blocks under near-source ground motions. Geotechnique 2000;50(3):243–62.

[26] Cremer C, Pecker A, Davenne L. Modelling of nonlinear dynamic behaviour of a shallow strip foundation with macro-element. J Earthq Eng 2002;6(2):175–211.

[27] Gazetas G, Apostolou M. Nonlinear soil–structure interaction: foundation uplifting and soil yielding. Proceedings of third joint United States–Japan workshop on soil–structure interaction, California; 2004.
[28] Gazetas G. Analysis of machine foundation vibrations: state of the art. Int J Soil Dyn Earthq Eng 1983;2:2–42.
[29] Veletsos AS, Wei YT. Lateral and rocking vibrations of footings. J Soil Mech Found Div ASCE 1971;97(9):1227–48.
[30] Luco JE, Westmann RA. Dynamic response of circular footings. Int Eng Mech Div ASCE 1971;97:1381–95.
[31] Randolph MF, Wroth CP. Analysis of deformation of vertically loaded piles. J Geotech Eng Div ASCE 1978;104(12):1465–88.